Optimal Linear Estimation of Binary Star Parameters

Daniel Burke[1], Nicholas Devaney[1], Szymon Gladysz [1],Harrison H. Barrett [2,3], Meredith K. Whitaker [2,3] and Luca Caucci [2,3]

[1]School of Physics, National University of Ireland Galway, Ireland;
[2]College of Optical Sciences,University of Arizona;
[3]Center for Gamma Ray Imaging,University of Arizona;

ABSTRACT

We propose a new post-processing technique for the detection of faint companions and the estimation of their parameters from adaptive optics (AO) observations. We apply the optimal linear detector, which is the Hotelling observer, to perform detection, astrometry and photometry on real and simulated data. The real data was obtained from the AO system on the 3m Lick telescope[1] .

The Hotelling detector, which is a prewhitening matched filter, calculates the Hotelling test statistic which is then compared to a threshold. If the test statistic is greater than the threshold the algorithm decides that a companion is present. This decision is the main task performed by the Hotelling observer. After a detection is made the location and intensity of the companion which maximise this test statistic are taken as the estimated values.

We compare the Hotelling approach with current detection algorithms widely used in astronomy. We discuss the use of the estimation receiver operating characteristic (EROC) curve in quantifying the performance of the algorithm with no prior estimate of the companion's location or intensity. The robustness of this technique to errors in point spread function (PSF) estimation is also investigated.

1. INTRODUCTION

The two main post processing techniques applied to AO observations of binary stars are PSF fitting[2,3] and blind deconvolution.[4,5] These algorithms return astrometry and photometry for a given binary star image. In this paper we propose to use the scanning Hotelling observer[6,7] , which is the optimal linear observer, to extract astrometry and photometry from real and simulated observations of binary star images. Throughout our study we have compared the extracted values from the Hotelling observer to the results obtained using the StarFinder code[3] . The Hotelling observer provides a framework to include spatial and temporal information about the image noise, as well as knowledge and statistics about the varying PSF. With the use of the receiver-operating-characteristic (ROC) curve we quantify the performance of the Hoteling observer. Our goal being to develop a rigorous approach to faint companion detection, localisation and intensity estimation.

In section 2 we review current post-processing algorithms which have been applied to the tasks of astrometry and photometry from AO images of binary stars. In section 3 the receiver-operating characteristic curve is introduced. This section also defines the figure of merit used to asses task performance. We also describe generalisations: the localisation receiver-operating characteristic (LROC) and the estimation receiver-operating characteristic (EROC) curves. Section 4 presents the Hotelling observer for the three tasks. Section 5 reports on simulation experiments carried out using the Hotelling observer and the StarFinder algorithm. This section concludes with the application of the Hotelling observer to real data from the Lick Observatory[8] . Our paper is concluded in section 6 with a discussion on the performance of the observer and some suggestions for future study.

Further author information: (Send correspondence to Daniel Burke.)
Daniel Burke: daniel.burke@nuigalway.ie, Telephone: +353 91 492984

Adaptive Optics Systems, edited by Norbert Hubin, Claire E. Max, Peter L. Wizinowich,
Proc. of SPIE Vol. 7015, 70152J, (2008)
0277-786X/08/$18 · doi: 10.1117/12.788973

2. CURRENT APPROACHES TO BINARY STAR PARAMETER ESTIMATION

The two main techniques which are currently in use for astrometry and photometry on adaptive optics (AO) observations are point spread function fitting[3] and deconvolution[4,5] . However there are several problems to be considered when applying these methods. Esslinger and Edmunds[9] defined the major sources of error as:

1. Global PSF changes between the science object and the reference PSF star
2. Inaccuracy in PSF estimation for deconvolution

The first error can be reduced by careful selection of the reference PSF star. The observer should try and match both stars in apparent magnitude and spectral type so that the level of AO correction is similar. Also the time delay between the reference PSF and science observations should be as small as possible[9] and preferably with the same air mass.

Barnaby *et al*[10] proposed to use two methods of photometry; Parametric Blind Deconcovolution (PBD) and Iterative Blind Deconvolution (IBD). In PBD the AO data is modelled as a fit for two stars, each with a two-dimensional function. A two-dimensional Lorentzian profile is convolved with two δ functions of amplitude $\mathscr{A}$. A nonlinear least squares fit is used to determine the PSF profiles and the error on each parameter is returned by the PBD method. The IBD technique sets out to minimise an error metric such that the estimated PSF profile fits that of the data set. Observations of a reference star are used as the initial estimate of the PSF. The algorithm is then allowed to converge. The reconstructed object is fitted with an elliptical Gaussian profile to determine the locations and amplitudes of the two sources in the image.

Diolaiti and Bendinelli[3] developed the StarFinder code which was initially intended for use on AO images of crowded stellar fields. But this code can also be used on AO images of binary stars. StarFinder assumes that the PSF is isoplanatic and that the PSF is Nyquist sampled. The observed image is modeled as a composition of scaled shifted replicas of the PSF. Initially, bright isolated stars in the crowded field are used as an estimate of the PSF. A star list is then generated by searching the image for relative maxima. These detected stars are then accepted/rejected based on their correlation coefficient with the estimated PSF. Relative photometry and astrometry are estimated by minimising the least square error between the observed image and the reconstructed image.

3. THE ROC CURVE AND ITS VARIANTS

When analysing an image of a binary star there are three decisions of interest which we want our observer/algorithm to make:

1. Detection → is a companion present?
2. Localisation → where is the companion in the image?
3. Photometric Estimation → what is the intensity of the companion?

When considering the detection task, there are four possible scenarios to this decision[11] . A *true positive* (TP), or a "hit", occurs when the observer concludes that a companion is present in the image when it really is present. A *false positive* (FP), or "false-alarm", is when a companion is deemed to be present when in fact it is absent. A *false negative* (FN), or "miss", arises when the observer decides that a companion is absent when it is actually present. A *true negative* (TN) is the correct report of the absence of a companion. The

observer's task is to decide between two hypotheses, H_0 the companion absent case and H_1 the companion present case. The true-postitive-fraction (TPF) for a test statistic t at a given threshold x is given by

$$TPF(x) = Pr(t \geq x|H_1) = \int_x^\infty dt\ pr(t|H_1). \tag{1}$$

The TPF can be thought of as the probability of a "hit" for a given threshold x. The false-positive-fraction (FPF), probability of "false-alarm", at a given threshold x is given by

$$FPF(x) = Pr(t \geq x|H_0) = \int_x^\infty dt\ pr(t|H_0). \tag{2}$$

The threshold x therefore controls the trade-off between the TPF and the FPF. Graphically, this is portrayed by the receiver-operating-characteristic (ROC) curve. The ROC curve, see figure 1, is a plot of TPF(x) versus FPF(x).

A common scalar figure of merit used is the area under the ROC curve denoted AUC[12] . An $AUC = 0.5$ corresponds to a worthless system and as a system approaches performing the task perfectly the $AUC \approx 1$. Therefore it is desirable to maximise the AUC. The area under the ROC curve[12] is given by

$$AUC = \int_0^1 TPF\ d(FPF) = -\int_\infty^\infty dx\ TPF(x)\ \frac{d}{dx}FPF(x). \tag{3}$$

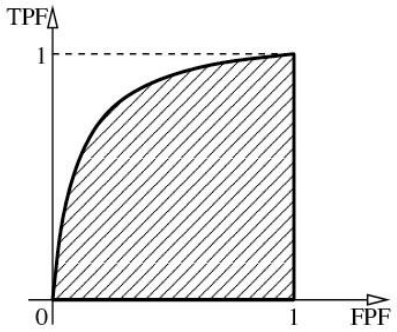

Figure 1: The ROC Curve for a hit-miss detection task

The localisation task can be combined with the detection task such that the observer also returns an estimate of the companion's location[13] . The TPF can now be defined as the probability of a correct detection combined with the probability of correctly localising the companion within a given tolerance, η, of the true location. The TPF-FPF plot for a detection and localisation task is called the localisation ROC (LROC) curve.

The LROC curve can be generalized into an estimation ROC (EROC) curve for an arbitrary estimation task[14] . This is how a photometry step can be added to the detection and localisation task. The TPF can now be defined as the probability of detecting a companion at a location within the given tolerance, η, of the true location and with its estimated magnitude within a given tolerance, ε, from the true magnitude.

4. THE HOTELLING OBSERVER

The optimal discriminant function, referred to as the ideal-observer, is the *likelihood ratio*:

$$\Lambda(g) = \frac{pr(g|H_1)}{pr(g|H_0)}, \tag{4}$$

where g is the data.

The probability density functions under both hypotheses are required in order to compute the ideal-observer. However in practice this information can be difficult to obtain a priori.

The *Hotelling Observer*[6] is the ideal-linear-observer. That being the case we use the Hotelling observer to perform the tasks of companion detection, astrometry and photometry. The Hotelling observer provides a framework to include spatial and temporal correlation information about the noise, as well as knowledge about the statistics of the random PSF. It calculates a linear discriminant of the form $t(g) = w^t g$, where w is called the template, g is the data and $t(g)$ is the test statistic. Let $\overline{g}_0$ denote the mean, noise free, image when the planet is absent. The single overbar denotes mean data averaged over noise. Let $\overline{g}_{1,r_{pl}}$ equal the mean, noise free, image when the planet is present at position r_{pl}. To compute the Hotelling test statistic, $t_{Hot}(g)$, knowledge of the overall mean data vectors, $\overline{g_1}$ and $\overline{g_0}$, and the covariance matrices, K_g, under both hypothes are needed. The Hotelling test statistic takes the form:

$$\begin{aligned} t_{Hot}(g) &= w^t g = [\overline{g_1} - \overline{g_0}]^t K_{av}^{-1} g, \\ \text{where } K_{av}^{-1} &= [\frac{1}{2}(K_{g|H_1} + K_{g|H_0})]^{-1}. \end{aligned} \tag{5}$$

Matrices $K_{g|H_1}$and $K_{g|H_0}$ denote the covariance matrices of the data under the planet present case H_1 and the planet absent case H_0. The Hotelling observer is sometimes referred to as a prewhitening matched filter[15] . In Caucci *et al*[7] assumptions are made such that an analytical expression for the inverse covariance matrix, K_g^{-1}, can be obtained. An analytical expression for $t_{Hot}(g)$ can then be derived. The authors first assume that the science object f is nonrandom and that a sequence of short exposure images, $g^{(J)}$, are processed to get a single long exposure image g. The desired signal is then $s_{r_{pl}} = \overline{g}_{1,r_{pl}} - \overline{g}_0$. Recalling the meaning of H_0 and H_1, the noisy images under the two hypotheses are given by:

$$H_0 : g = \overline{g}_0 + n, \qquad H_{1,r_{pl}} : g = \underbrace{\overline{g}_0 + s_{r_{pl}}}_{\overline{g}_{1,r_{pl}}} + n. \tag{6}$$

The noise n is composed of Gaussian noise from the detector readout and Poisson noise from detection of the incident radiation. The noise in different pixels is uncorrelated, if this were not the case K_g would not be diagonal. In the following we denote $h_m(r)$ as the m-th pixel of the dicretised version of the long-exposure PSF; A_* as the intensity of the parent star, located at r_*; a_{pl} the intensity of the companion, located at r_{pl}; b_m as the background intensity and σ_m^2 as the variance of the detector readout noise at the m-th pixel. The mean images are then:

$$\overline{g}_{0,m} = Ah_m(r_*) + b_m, \qquad \overline{g}_{1,m} = Ah_m(r_*) + a_{pl}h_m(r_{pl}) + b_m. \tag{7}$$

Additional assumptions are needed to attain an analytical form of K_g. The long-exposure PSF must be nonrandom and known, speckle noise must be removed or reduced and K_g is assumed to be equal under both hypotheses. The last assumption is valid as long as $s_{r_{pl}} \ll \overline{g}_0$. It should be stated that for a series of short exposure images K_g cannot be given an analytical form. With these assumptions K_g is a diagonal matrix. Then, knowing that the elements on the diagonal are variances (and so strictly positive) it follows that K_g^{-1} is diagonal. The diagonal elements of K_g are given by:

$$[K_g]_{m,m'} = [Ah_m(r_*) + b_m + \sigma_m^2]\delta_{m,m'}. \tag{8}$$

Where $\delta_{m,m'}$ is the Kronecker delta function. Substituting this expression for K_g back into equation 5 we get:

$$t_{Hot}(g|r_p) = \sum_{m=1}^{M} w_m g_m = \sum_{m=1}^{M} \frac{a_{pl}h_m(r_{pl})}{Ah_m(r_*) + b_m + \sigma_m^2} g_m. \tag{9}$$

This form of the Hotelling observer is the optimal linear observer in detection problems when the signal location r_p, intensity a_{pl}, background, b_m, and the PSF, $h_m(r)$, are known.

When the companion's location, r_{pl}, is unknown a set of test locations T can be defined to introduce a scanning observer[15,16] . The ideal-observer (equation 4) is at a maximum at the companion location, $r_{pl} \in T$. The ideal-observer now takes on the form

$$\Lambda(g) = \max_{r_{pl} \in T} \Lambda(g|r_{pl}) = \max_{r_{pl} \in T} \frac{pr(g|H_1, r_{pl})}{pr(g|H_0)}. \tag{10}$$

The estimation of r_{pl} is then computed as

$$\widetilde{r_{pl}} = \arg \max_{r_{pl} \in T} \Lambda(g|r_{pl}). \tag{11}$$

The likelihood ratio (equation 10) can be evaluated[13] by assuming that the densities $pr(g|H_1, r_{pl})$ and $pr(g|H_0)$ can be approximated by Gaussian distributions. In a similar manner to the derivation of equation 9 we can get expressions for the optimal linear observer and the estimated companion location $\widetilde{r_{pl}}$, when r_{pl} is unknown. It should be noted that some terms were discarded in the derivation of equation 9 but cannot be disposed of in this derivation. This is because the location of the companion, r_{pl}, affects the location of the maximum value of $t_{Hot}(g, r_{pl})$. The scanning Hotelling observer now takes the form:

$$t_{Hot}(g, r_{pl}) = \sum_{m=1}^{M} w_m g_m = \sum_{m=1}^{M} \frac{a_{pl} h_m(r_{pl})}{A h_m(r_*) + b_m + \sigma_m^2} \; [g_m - \overline{g}_{0,m} - \frac{1}{2} a_{pl} h_m(r_{pl})]. \tag{12}$$

The companion intensity a_{pl} is assumed known. The estimation of the companion's position $\widetilde{r_{pl}}$ is then defined as:

$$\widetilde{r_{pl}}(g) = \arg \max_{r_{pl} \in T} [t_{Hot}(g, r_{pl})]. \tag{13}$$

In the following equation 13 is referred to as the Spatial Scanning Hotelling Estimator (SSHE). An additional step is now required to scan not only spatially for the companion, but to also scan in intensity for the companion. The scanning Hotelling observer can then estimate a_{pl}. Clarkson[14] showed that a maximum likelihood estimate is close to optimal in the EROC sense when a narrow tolerance is allowed. The ideal EROC observer is defined as:

$$T_1(g) = \max_{\theta} \{\Lambda(g|\theta)\}, \tag{14}$$

$$\widetilde{\theta}(g) = \arg \max_{\theta} \{pr(g|\theta, H_1)\}. \tag{15}$$

θ represents a vector of parameters associated with the companion signal. We want an estimate of the signal location and intensity. Choosing $\theta = (r_{pl}, a_{pl})$ and defining a set of test intensities I, θ varies over the Cartesian product of T and I. The spatial scanning Hotelling observer (equation 12) becomes a spatial-intensity scanning observer of the form

$$t_{Hot}(g; r_{pl}, a_{pl}) = \sum_{m=1}^{M} \frac{a_{pl} h_m(r_{pl})}{A h_m(r_*) + b_m + \sigma_m^2} \; [g_m - \overline{g}_{0,m} - \frac{1}{2} a_{pl} h_m(r_{pl})]. \tag{16}$$

Equation 16 differs from equation 12 in that the maximum of the test statistic, $t_{Hot}(g; r_{pl}, a_{pl})$, is now dependent upon r_{pl} and a_{pl} and not just upon r_{pl}. The estimation of θ is then defined as:

$$\widetilde{\theta}(g) = \arg \max_{\theta \in T \times I} [t_{Hot}(g; r_{pl}, a_{pl})]. \tag{17}$$

We refer to this estimator as the Maximised Hotelling Estimator (MHE).

The companion intensity can be linearly related to the companion signal, $s(r_{pl}) = a_{pl}h_m(r_{pl})$. This is the case once the binary companion has been detected and located in an image i.e. r_{pl} is known. Recall the scanning Hotelling observer takes the form:

$$t_{Hot}(g, r_{pl}) = s^t K_g^{-1}(g_m - \overline{g_0}) - \frac{1}{2}s^t K_g^{-1} s. \tag{18}$$

The estimate of a_{pl} then becomes[17]

$$\begin{aligned} \widetilde{a_{pl}} &= \arg\max_{a_{pl}}\{s^t K_g^{-1}(g_m - \overline{g_0}) - \frac{1}{2}s^t K_g^{-1} s)\}, \\ &= \arg\max_{a_{pl}}\{a_{pl}h_m(r_{pl})^t K_g^{-1}(g - \overline{g_0}) - \frac{a_{pl}^2}{2}h_m(r_{pl})^t K_g^{-1} h_m(r_{pl})\}. \end{aligned} \tag{19}$$

These terms are maximised at the estimate, leading to

$$\begin{aligned} \widetilde{a_{pl}} &= \frac{h_m(r_{pl})^t K_g^{-1}(g_m - \overline{g}_0)}{h_m(r_{pl})^t K_g^{-1} h_m(r_{pl})}, \\ &= \frac{h_m(r_{pl})^t (A h_m(r_*) + b_m + \sigma_m^2)(g_m - \overline{g}_0)}{h_m(r_{pl})^t (A h_m(r_*) + b_m + \sigma_m^2) h_m(r_{pl})}. \end{aligned} \tag{20}$$

This is an unbiased estimator i.e. the estimated value of a_{pl} equals the true value when averaged over noise and background. We refer to equation 20 as the Optimal Hotelling Estimator (OHE).

5. EXPERIMENTAL RESULTS

Over the course of this study we tested the performance of the Hotelling observer in a variety of different observational situations. In all cases the AUC of the ROC curve was used as the figure of merit to quantify the observer performance.

5.1 Simulation Results

To test the photometric accuracy of the proposed approached vs. PSF-fitting we used moderate-Strehl ratio (SR) data obtained using the Lick Observatorys AO system.[1] Closed loop images of bright single stars were obtained using the high-speed sub-array mode with a size of 64×64 pixels of the 256×256 pixel IRCAL camera[18] . This corresponds to field size of 4.864×4.864 arcseconds. The sub-array measurements were captured with typical exposure times of 22ms. Each dataset comprised ten thousand images. All data were obtained in the two-micron (K) band where the diffraction-limit is 151mas so that the data is effectively Nyquist sampled. The observations were made close to the zenith and using the highest possible closed-loop frame rate. The individual short exposures were registered with sub-pixel accuracy to produce shift-and-add (SAA) images. The measured Strehl ratios in these SAA images were in the range $0.25 - 0.55$. For the details of the observations and data reduction see Gladysz *et al*[8] .

We used three SAA images corresponding to the same star (HD 153832 $m_V = 7.25, m_K = 4.78$, spectral type K0), observed continuously for one hour. The three datasets were observed one after the other, but due to variable "seeing" the Strehl ratios of the SAA images were 0.49, 0.43, and 0.42. These SAA images formed the input for the MHE (equation 12), the OHE (equation 20) and the StarFinder PSF-fitting package. We simulated two general cases: properly-matched PSFs (0.43 and 0.42 SR pair), and mismatched PSFs (0.49 and 0.42 SR pair). Artificial binaries ($\Delta m_K = 3.5$ or 4.5, separation $\theta = 0.6$") were simulated by scaling and shifting the 0.42-Strehl ratio image. To include the variability induced by the presence of the static speckles for each of the four cases (table 1) we tested eight locations for the companion (figure 2). In all cases the OHE had the smallest photometric error. The MHE and StarFinder produced comparable photometry.

We also used an end-to-end IDL-based package called PAOLA (Performance of Adaptive Optics for Large/Little Apertures)[19] to simulate the PSF of the Lick telescope. The main difference between the two

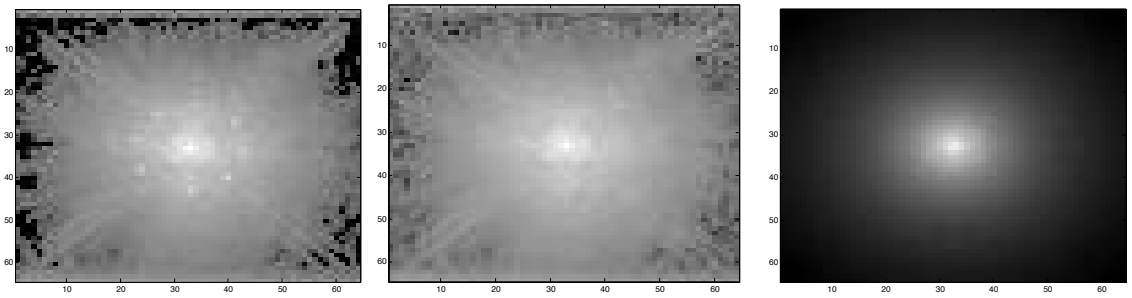

(a) Eight different companion locations (log scale) **(b)** Lick PSF (log scale) **(c)** PAOLA PSF (log scale)

Figure 2: Artificial Binary Star Locations and the two different PSF's used in creating the artificial binary star data. (Log scale)

PSFs is that the "real" Lick PSF contains residual structure in the halo of the PSF. This structure is probably due to the telescope's spider arms and some static speckles. The PAOLA generated PSF's are essentially clean in regard to this residual structure. This difference is evident from figure 2 where of the PSFs have the same Strehl ratio.

Table 1: Comparative photometry estimation test.

Δm	**PSF**	**Mean $\lvert\Delta\widetilde{\mathbf{m}} - \Delta\mathbf{m}\rvert$**		
		MHE [a]	OHE[b]	StarFinder
3.49	Good	0.12	0.05	0.14
	Bad	0.26	0.08	0.25
4.5	Good	0.25	0.14	0.3
	Bad	0.57	0.22	0.61

[a] MHE refers to equation 17
[b] OHE refers to equation 20

The combined detection-localisation task is carried out in the following manner. Poisson and Gaussian noise is added to each image under consideration, such that each realisation of the data will be statistically independent. For each test location (see figure 3) the spatial scanning Hotelling observer (equation 12) calculates its test statistic, $t_{Hot}(g, r_{pl})$. This set of test statistics is then at a maximum at the estimated location of the companion, i.e. at r_{pl}. The LROC curve is then built up by generating multiple realisations of the data and scanning each image. This results in a set of $(\widetilde{r_{pl}}, t_{hot}(g, \widetilde{r_{pl}}))$ pairs for each image scanned. The TPF for this test is defined as a correct detection (at a given threshold) with $\widetilde{r_{pl}} < |r_{pl} + \eta|$, where η equals a single pixel. As described in section 3 the threshold is then varied to graphically map out the *true positive fraction* versus *false positive fraction*, i.e. the LROC curve. The combined detection-localisation task was carried out for a range of different companion separations and magnitudes relative to the primary, (see figure 4).The AUC under the LROC curve is denoted ALROC.

The combined detection-localisation-estimation task is performed in a similar fashion. For each test location in figure 3 the spatial-intensity scanning Hotelling observer (equation 16) calculates the test statistic for a set of test intensities. This three dimensional set of test statistics is at a maximum at the location of the companion, r_{pl}, and at the intensity of the companion, a_{pl}. As in the LROC curve case each realisation of the data results in a single test statistic and pair of estimates i.e. $(\widetilde{r_{pl}}, \widetilde{a_{pl}}, t_{hot}(g; \widetilde{r_{pl}}, \widetilde{a_{pl}}))$. The TPF for this

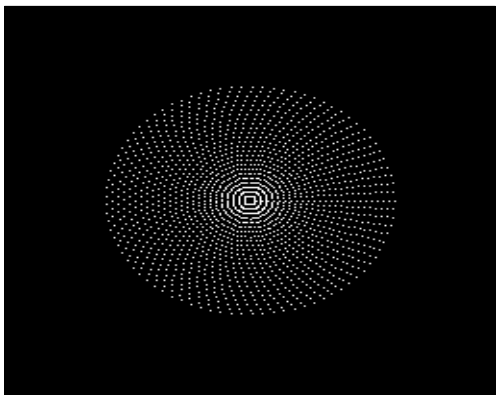

Figure 3: The set of test locations for the scanning Hotelling observer

test is defined as a correct detection (at a given threshold) with $\widetilde{r_{pl}} < |r_{pl} + \eta|$, where η equals a single pixel, and $\widetilde{a_{pl}} < |a_{pl} + \varepsilon|$, where ε equals 0.1 magnitudes. For multiple realisations of the data an EROC curve is generated. The performance of the MHE in estimating the companion's intensity, a_{pl}, was compared to the OHE. The advantage of the OHE over the MHE is that there is no need to scan over a range of test intensities. This estimation task was carried out for a range of companion separations and magnitude differences, see figure 5. The AUC under the EROC curve is called the AEROC.

The robustness of these two tasks was assessed by mismatching the PSF used in creating the data and the PSF used in the scanning Hotelling observers. The PAOLA package was used to create the data for this experiment. The results of these tests are presented in figure 6. This test was carried out over three ranges of Strehl ratio: $30 \rightarrow 40$, $50 \rightarrow 60$ and $70 \rightarrow 80$. The result from the low Strehl ratio test suggests that the observer is more accurate when the Strehl ratio is over estimated. However the error at higher Strehl ratio was observed to be symmetric about the true Strehl ratio.

5.2 Application to Real Observations

Observations of SAO 83636 were also available, as well as the data from Gladysz *et al*[8] . This third binary was observed using the Lick Observatorys AO system[1] and reduced in the same manner as in[8] . These three data sets (see figure 7) were analyzed using both the Hotelling estimators and StarFinder. The results of these analyses are presented in table 2. The astrometry from StarFinder and the MHE were very similar for the three systems. There is a difference of up to 0.2 mag in photometry between the three observers (SF, MHE, OHE). However the OHE has the smallest error in table 1 and therefore it would be reasonable to assume this estimator is also closest to the true value of Δm_K here. It should be noted that there is no quoted Δm for the three observed systems in the K band.

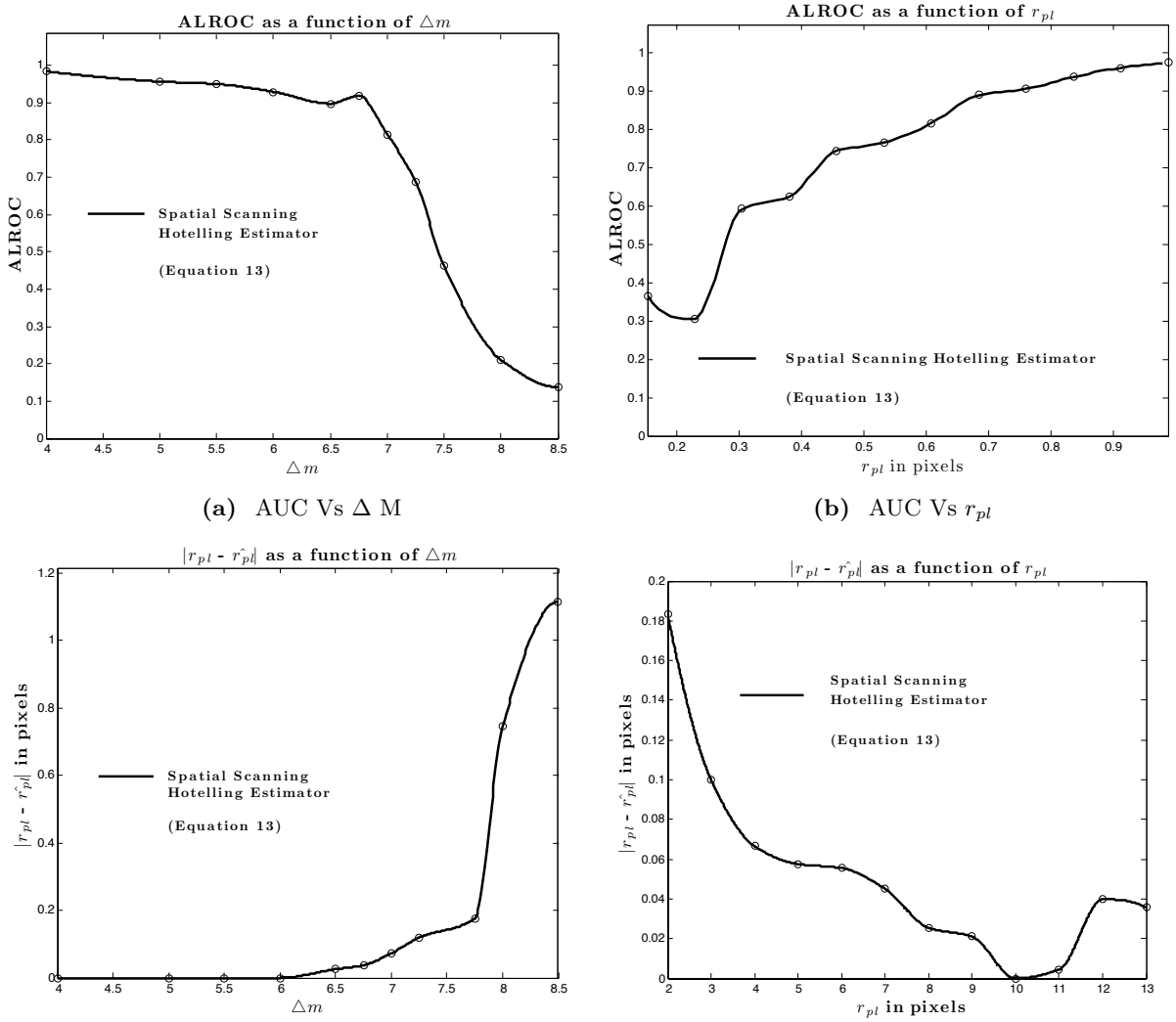

(a) AUC Vs Δ M

(b) AUC Vs r_{pl}

(c) Error Vs Δ M

(d) Error Vs r_{pl}

Figure 4: Area Under LROC Curves for a range of different companion separations and magnitudes and the error on $\widetilde{r_{pl}}$ associated with these values

6. SUMMARY

Our current implementation of the Hotelling observer extracts photometry, (OHE), with an error three times smaller than that of StarFinder (see table 1). Astrometry is also calculated with similar accuracy to other algorithms in use (see table 2). This is verified from experiments using simulated binary star images. We note that comparative observer tests showed that the OHE (equation 20) has a much smaller error in estimating the companion's intensity than both the MHE and the StarFinder code. The reason for this performance gap is not clear as of yet. Investigations to determine this discrepancy are underway.

We have carefully assessed our observer's task performance at each stage of the estimation process. The structure of this task assessment has been based around the use of the ROC curve and its figure of merit the area under the ROC curve and generalisations.

The application of the Hotelling observer to real binary star image data confirmed the reliability of the observer. The values for astrometry and photometry were relatively close to those produced by StarFinder.

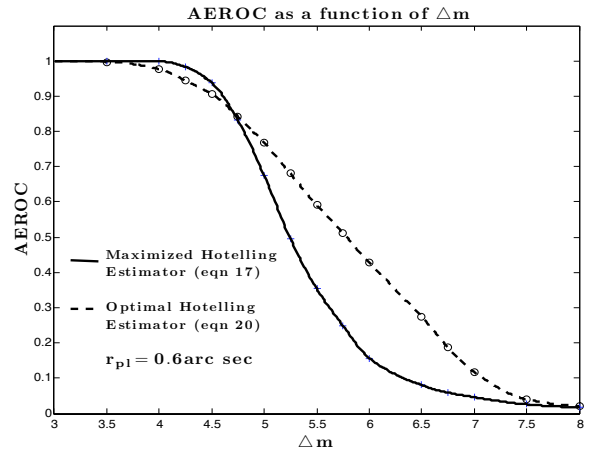

(a) AUC Vs Δ M

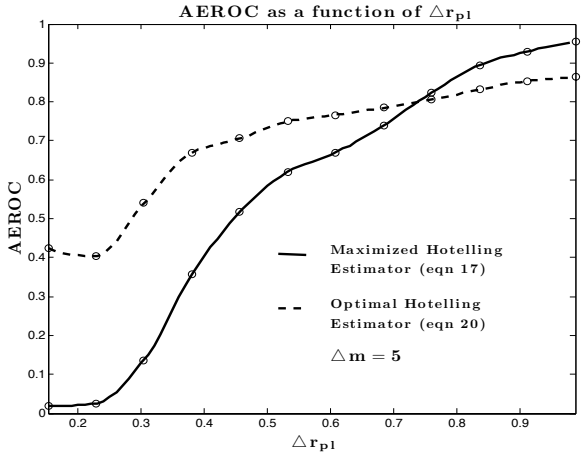

(b) AUC Vs r_{pl}

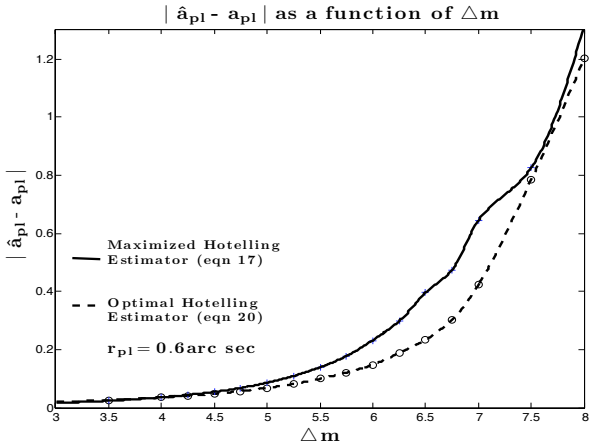

(c) Error Vs Δ M

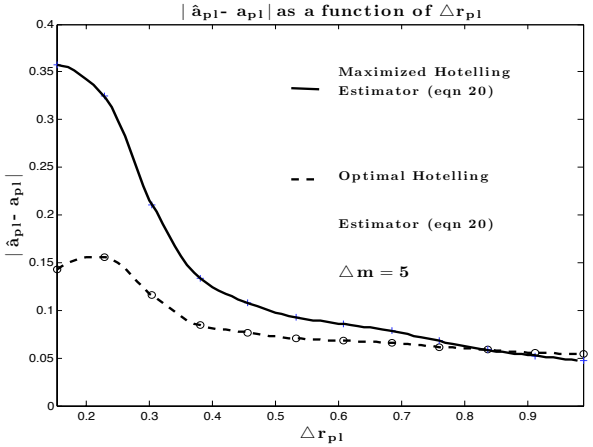

(d) Error Vs r_{pl}

Figure 5: Area Under EROC Curves for a range of different companion separations and magnitudes and the error on $\widetilde{a_{pl}}$ associated with these values.

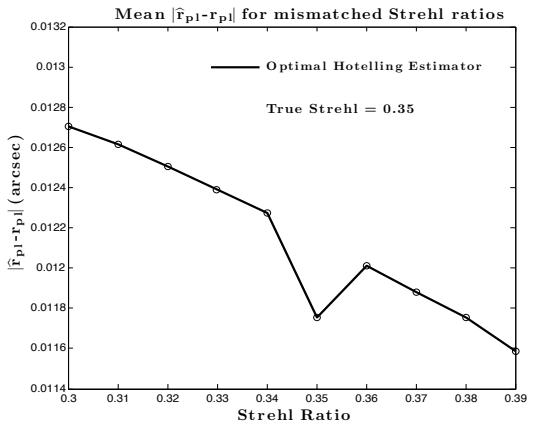

(a) Detection-Localisation Task

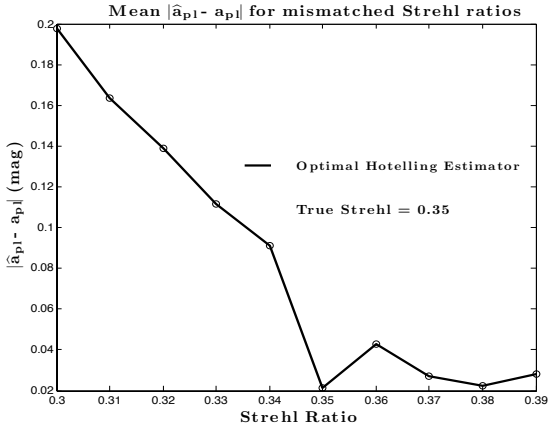

(b) Combined Detection-Estimation Task

Figure 6: Robustness of the two estimation tasks

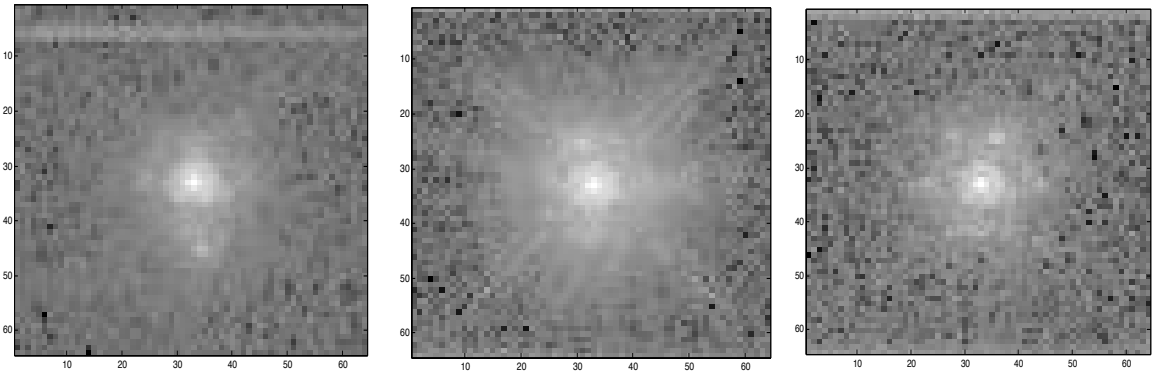

(a) SAO 83636 **(b)** HD 235089 **(c)** HD 170648

Figure 7: Three binary systems analysed with Hotelling and StarFinder algorithms (plotted on log scale)

Table 2: Quoted and estimated system parameters for three observed binaries using both Hotelling Estimators and StarFinder.

Name	**Quoted Sep.(WDS[20])**	**Estimated Sep.**	**Quoted Δm_V**	**Estimated Δm_{Ks}**
SAO 83636	1 arcsec	0.912 arc second (MHE[a])	6.5	3.4 (MHE)
		0.924 arcsec (SF[b])		3.18 (SF)
				3.18 (OHE[c])
HD 235089	0.4 arcsec	0.584 arc second (MHE)	3.7	3.93 (MHE)
		0.586 arcsec (SF)		3.95 (SF)
				4.06 (OHE)
HD 170648	0.8 arcsec	0.692 arc second (MHE)	4.2	3.07 (MHE)
		0.69 arcsec (SF)		3.03 (SF)
				3.17 (OHE)

[a] MHE refers to equation 16
[b] SF: StarFinder
[c] OHE refers to equation 20

For our Lick data, the computation time needed for the Hotelling observer to scan a 3×3 neighbourhood is about 17 seconds. However StarFinder yields results in less than a second. In the future we plan to optimize the companion location estimation task (equation 13) through the use of a gradient minimization routine. This optimization will reduce the set of test locations, T, to a minimum. Accordingly the execution time of the MHE should also reduce to a minimum.

At present neither the Hotelling observer nor StarFinder can distinguish between the presence of static speckles and that of a companion. Gladysz & Christou[21] have proposed a technique which partially removes the static speckles, smoothing out the outer regions of the AO-corrected PSFs. In the future we plan to combine this technique with the Hotelling observer.

In conclusion we have used the Hotelling observer to develop a rigorous approach to the detection, localisation and photometric estimation of binary star companions. In the future with the optimization of the Hotelling observer we will be able to characterise binary systems with larger relative magnitudes and closer separations than are presented here.

7. ACKNOWLEDGMENTS

This research was funded by Science Foundation Ireland Grant No. 07/IN.1/I906. The authors wish to acknowledge the SFI/HEA Irish Centre for High-End Computing (ICHEC) for the provision of computational facilities and support.

REFERENCES

[1] B.J.Bauman, Gavel, D., and K.E.Waltjen, "New optical design of adaptive optics system at lick observatory," *Proc. SPIE* **3762**(194-200) (1999).

[2] Eaton, N. and Privett, G., "http://www.starlink.rl.ac.uk/star/docs/sun42.htx/sun42.html," (Dec. 1996).

[3] E.Diolaiti and O.Bendinelli, "Analysis of isoplanatic high resolution stellar fields analysis of isoplanatic high resolution stellar fields by the starfinder code," *Astronomy and Astrophysics, Supplimentary Series* **147**, 335–346 (2000).

[4] ten Brummelaar and B.Mason, "Binary Star Differential Photometry Using the Adaptive Optics System at Mount Wilson Observatory," *AJ* **119**, 2406–2414 (May 2000).

[5] L.Roberts, N.Turner, L.Bradford, Brummelaar, T., and B.Oppenheimer, "Adaptive optics photometry and astrometry of binary stars," *AJ* **130**, 2262–2271 (Nov 2005).

[6] Barrett, H., J.Denny, Wagner, and Myers, "Objective assessment of image quality. II. fisher information, fourier crosstalk, and figures of merit for task perfomance," *JOSA A* **12** (May 1995).

[7] L.Caucci, H.Barrett, N.Devaney, and J.Rodriguez, "Application of the hotelling and ideal observers to detection and localization of exoplanets," *JOSA* **24**(12), B13–B24 (2007).

[8] Gladysz, S., Christou, J. C., and Refern, M., "Characterization of the lick adaptive optics point spread function," *Proc. SPIE* **6272** (2006).

[9] O.Esslinger and Edmunds, "Photometry with adaptive optics: A first guide to expected performance," *Astronomy and Astrophysics, Supplimentary Series* **129**, 617–635 (1998).

[10] D.Barnaby, E.Spillar, J.Christou, and J.Drummond, "Measurments of binary stars with the starfire optical range adaptive optics systems," *AJ* **119**, 378–389 (Jan 2000).

[11] H.Barrett and K.Myres, [*Foundations of Image Science*], Weily Series in Pure and Applied Optics (2004).

[12] H.Barrett, C.Abbey, and E.Clarkson, "Objective assessment of image quality. III. roc metrics,ideal observers, and likelihood generating functions," *JOSA* **15**(6) (1998).

[13] Caucci, L., *Point Detection and Hotelling Discriminant: An Application In Adaptive Optics*, Master's thesis, Dept. Electrical and Computer Engineering, The University of Arizona (2007).

[14] Clarkson, E., "Estimation receiver operating characteristic curve and ideal observers for combined detection/estimation tasks," *JOSA A* **24** (December 2007).

[15] H.Barrett, K.Myres, N.Devaney, and C.Dainty, "Objective assessment of image quality.IV. application to adaptive optics," *JOSA* **23**(12) (2006).

[16] L.Caucci, H.Barrett, N.Devaney, and J.Rodriguez, "Statistical decision theory and adaptive optics," *OSA* (June 2007).

[17] Whitaker, M. K., Clarkson, E., and Barrett, H. H., "Estimating random signal parameters from noisy images with nuisance parameters: Linear and scanning-linear methods," *Optics Express* **16** (May 2008).

[18] M.P.Fitzgerald and J.R.Graham, "Speckle statistics in adaptively corrected images," *AJ* **637**, 514–547 (2006).

[19] Jolissaint, Véran, and Conan, "Analytical modeling of adaptive optics: foundations of the phase spatial power spectrum approach," *JOSA* **23** (Feb. 2006).

[20] "The washington double star catalog, http://ad.usno.navy.mil/wds/," (May 2008).

[21] Gladysz, S. and Christou, J. C., "Reference-less detection, astrometry, and photometry of faint companions with adaptive optics," *In Preperation* (2008).